A UGV-Based Forest Vegetation Optical Depth Mapping Using GNSS Signals

Abesh Ghosh, *Student Member, IEEE*, Md Mehedi Farhad, *Student Member, IEEE*, Dylan Boyd, *Member, IEEE*, and Mehmet Kurum, *Senior Member, IEEE*

***Abstract*—In this study, we conducted an empirical investigation on mobile global navigation satellite system (GNSS) transmissometry (GNSS-T) measurements to explore vegetation optical depth (VOD). Our approach involved using a dual-receiver setup, with one receiver located in open terrain to capture direct signals as a reference and another deployed on an unmanned ground vehicle (UGV) to sample vegetation across expansive forested regions. Noteworthy findings reveal the negligible influence of ground multipath effects within these forested terrains, effectively resulting in sampling the forest canopy rather than the ground itself as the receiver moves. The UGV-based method also uncovers VOD fluctuations inside the forest, offering insights into spatial distribution and the influence of satellite position on VOD measurements. The study further examines the effect of tree heterogeneity and seasonal dynamics on the VOD estimates. This empirical study contributes to our understanding of the VOD mapping capabilities of the mobile GNSS-T approach and can potentially lead to nonintrusive quantification of vegetation water content at a landscape scale in forest terrains. These results are significant for advancing our knowledge of forest ecosystem dynamics and sustainable resource management.**

***Index Terms*—Global navigation satellite system transmissometry (GNSS-T), soil moisture, unmanned ground vehicle (UGV), vegetation optical depth (VOD), vegetation water content (VWC).**

I. Introduction

FOREST areas are essential to the health of our environment and the development of civilization in general. All terrestrial ecosystems and climate change are greatly impacted by the distribution and productivity of vegetation [1], [2], [3]. There have been abrupt changes in phenology and vegetation productivity as a result of the increasing frequency and intensity of climate extremes, including both wet and dry conditions [4]. Droughts are becoming more severe, harsh, and frequent as the climate continues to warm [5]. The manner in which forests react to drought is influenced by various factors, including the flow and distribution of water in the soil-plant-atmosphere continuum [6]. There is significant evidence that vegetation water content (VWC) can serve as a useful measure of water status as it is directly linked to the moisture content of living fuel [1]. Improved temporal and spatial quantification of VWC variations is expected to aid in the improved evaluation of how forests respond to drought, including tree mortality and wildfire risk. Direct measurement of VWC dynamics remotely can also be crucial for understanding and modeling hydrological and ecological processes [7].

Assessing vegetation water characteristics typically necessitates extensive fieldwork, often involving the destruction of trees as indicated by [8]. Another common VWC estimation technique is using vegetation reflectance as a proxy [1]. While most vegetation indexes can be obtained at a high spatial resolution, atmospheric factors frequently compromise their effectiveness, leading to potential misinterpretations. In addition, these indexes lack a robust physics-based connection with the water content and have limited validity [9]. For instance, 1) the relationship between normalized difference vegetation index (NDVI) and VWC is empirical and plant-specific, and it depends on chlorophyll content; 2) changes in greenness do not always correspond to changes in VWC; 3) NDVI can quickly reach saturation levels at low-to-moderate VWC values. Despite these limitations, NDVI remains widely used in various applications due to its widespread availability [10].

Vegetation optical depth (VOD) has recently emerged as a new proxy to sense the VWC [11], [12], [13], [14], [15], [16], [17], [18], [19]. VOD is a parameter that quantifies the attenuation of microwave signals when traversing the above-ground vegetation canopy. It is a dimensionless quantity, with higher values indicating more attenuation and, hence, a larger quantity of VWC. VOD serves as an indicator of both the VWC and structure of the vegetation, offering valuable insights into the microwave interaction with the plant cover. The above-ground biomass (AGB) of a forest ecosystem is intricately linked to both its VWC and VOD, forming a critical nexus that contributes to our comprehensive understanding of ecological dynamics [1]. The correlation between microwave observables, specifically backscatter and VOD, and VWC is expounded upon in [11].

Manuscript received 15 October 2023; revised 7 January 2024; accepted 9 February 2024. Date of publication 14 February 2024; date of current version 23 February 2024. This work was supported in part by the Jet Propulsion Laboratory, California Institute of Technology, under a contract with the National Aeronautics and Space Administration under Grant 1683208, and in part by the NASA FINESST under Grant 80NSSC23K1553. *(Corresponding author: Mehmet Kurum.)*

Abesh Ghosh and Mehmet Kurum are with the School of Electrical and Computer Engineering, The University of Georgia, Athens, GA 30602 USA (e-mail: ag31608@uga.edu; kurum@uga.edu).

Md Mehedi Farhad is with the Department of Electrical and Computer Engineering, Mississippi State University, Mississippi, MS 39672 USA (e-mail: mf1413@msstate.edu).

Dylan Boyd is with the NASA Goddard Space Flight Center, Greenbelt, MD 20770 USA (e-mail: Dylan.R.Boyd@nasa.gov).

Digital Object Identifier 10.1109/JSTARS.2024.3365798

VOD observations became available globally through the opportunistic use of existing spaceborne measurements initially intended for other scientific purposes [20], [21], [22], [23], [24], [25]. VOD derived from both active and passive microwave observations is increasingly used for monitoring vegetation parameters, including VWC and AGB, across different frequency bands ranging from L to Ka bands [12], [16], [17], [25], [26]. Konings et al. [21] applied the multitemporal dual-channel algorithm to retrieve VOD from the first full year of soil moisture active passive (SMAP) L-band radiometric observations. Leveraging both the soil moisture and ocean salinity (SMOS) and the advanced microwave scanning radiometer for EOS (AMSR-E) measurements, a sensitivity analysis on soil moisture variations in the Bermejo basin, Argentina, comparing L-band SMOS measurements with C and X-band AMSR-E and highlighting the superior performance of lower frequencies in moderately dense forests have also been performed [25]. In addition, several studies done using the L-band SMOS data have shown good correlation between VOD and AGB, tree height and plant area index (PAI) [27], [28], [29], [30], [31]. Furthermore, the cyclone global navigation satellite system (CyGNSS) mission has been harnessed for AGB retrieval across diverse forest types, including rainforests, coniferous forests, dry forests, and moist tropical forests [32] [33].

Validating such spaceborne VOD products poses a significant challenge due to the lack of systematic ground-based VOD observations at the moment [34]. The availability of reliable VOD/VWC measurement in landscape scales also holds promises to provide ground truth for satellite-based VOD observations and extend isolated and time-consuming in-situ (often time-destructive) measurements of vegetation characteristics, such as biomass and VWC. Recently, a new methodology called the GNSS transmissometry (GNSS-T) technique has gained attention to monitoring VWC directly. The method uses stationary [35], [36], [37], [38], [39] or mobile [40], [41] GNSS receivers under the forest canopy, accompanied by an additional stationary unit in the open area as reference. The logarithmic difference between the two measurements yields information on forest transmissivity (water content). This relatively new remote sensing (nonintrusive) approach could transform forest VWC monitoring studies. Its optimal interpretation, use, and relation to VWC have yet to be comprehensively explored.

Point measurements [35], [36], [37], [38], [39] can be obtained by accumulating data over a long time at a single point. Such temporal measurements can help to resolve the contributions coming from different parts of the canopy. The point measurements can also capture variability in plant water status at diurnal timescales and resolve vegetation's dynamic physiological response to water stress [42]. However, extending such measurements to the landscape scale (e.g., 1 km) is not well understood since a spatially aggregated estimate is difficult, mainly due to extensive heterogeneity at the landscape scale. To scale the point measurements to larger spatial areas, we conducted coordinated field experiments involving mobile GNSS units under the forest canopy. Given the significant variations of VWC and relative water content within different tree components and across species, the result can inform the variability of VOD at a landscape scale. The spatial integration could help to average the heterogeneity and to resolve dynamics linked to soil water dynamics [43].

This article presents the development of a unique measurement system that utilizes an unmanned ground vehicle (UGV) for assessing VOD within forested areas. The primary objective of this research is to comprehensively characterize VOD across forest landscapes efficiently. By doing so, it aims to investigate sizeable forested regions in a relatively short time frame, offering insights into spatial variations within the forest environment and shifts in topography. To achieve these goals, a UGV equipped with a GNSS receiver featuring a linear antenna was employed. As the UGV navigates through the forested terrain, it captures attenuated signals through its receiver, storing the acquired data within its onboard computer storage. Concurrently, a second receiver configured identically is positioned within an unobstructed open area, receiving direct signals from GNSS satellites. The difference between the direct signals in the open space and the attenuated signals beneath the forest canopy is utilized to determine VOD. This method capitalizes on the inverse relationship between signal strength and VOD as well as VWC in a given area.

The UGV's path was strategically planned to traverse diverse tree zones, enabling the analysis of signals with respect to tree size and species. Consequently, this allows for a more nuanced analysis of how different tree types impact VOD measurements. In addition, the research incorporated data collected across different months to elucidate long-term or seasonal fluctuations in VOD. In summary, this study introduces a novel UGV-based VOD measurement system for comprehensive forest analysis. By considering diverse forest regions, tree species, and temporal variations, the research enhances our understanding of VOD dynamics and its correlation with satellite positioning in forested environments.

The rest of this article is organized as follows: Section II describes the methodology, which gives the theoretical background of the research, describes the site of the experiment, and reports the hardware that has been prepared for the experiment and the data collection procedure. Section III presents and evaluates the experimental results, and the implications of the findings are discussed. Finally, Section IV concludes this article.

II. Methodology

A. Measurement Configuration

The presence of forest vegetation has a notable influence on microwave signals, particularly GNSS signals in the L-band frequency range. As these signals penetrate through trees, they engage with the moisture contained in the leaves, branches, and trunks of the vegetation. The interaction causes signal attenuation and scattering, reducing the signal power passing through the vegetation canopy. It can be possible to determine the water content of the vegetation layer lying above the ground by examining the degree of signal degradation.

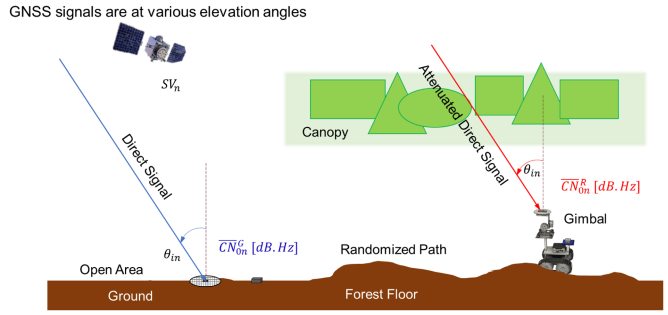

Fig. 1. Concept illustration of GNSS-T depicts two units: the reference unit (left), the forest unit, which can be integrated into a mobile robot for spatial sampling (right).

In order to measure the changes in signal strength, a GNSS transmissometry (GNSS-T) system is used in which a GNSS receiver is deployed in an open area to obtain a reference signal. This receiver directly captures signals transmitted by GNSS satellites and determines the unobstructed received signal strength. Simultaneously, another GNSS receiver with an identical configuration (forest or mobile unit) is placed inside the forest mounted on a UGV to capture the attenuated signal within the forested environment as illustrated in Fig. 1.

The antenna in the forest unit should be mounted on a metallic mesh to block signals reflected from the robot and the ground. Such a structure can be attached on the top of an inverted gimbal system (for the mobile platform) to align the direction and level of the antenna with respect to the one in the open sky. This configuration is carefully chosen to mitigate antenna-related degradation between two measurements.

While Fig. 1 showcases a single satellite, it is important to note that the four primary GNSS constellations host over one hundred satellites. At any given moment, approximately 30 or more satellites are visible, enabling comprehensive scanning of the majority of the upper hemisphere view of the antenna.

In this configuration, the direct (reference) signal measured by the reference unit of Fig. 1 can be written by

$$\mathrm{CN}_{0,p}^{G,n} = K_n G_{R,p}\left(\theta_{i,n}, \phi_{i,n}\right) \tag{1}$$

where $\mathrm{CN}_{0,p}$ represents the carrier-to-noise ratio that is a measure of the received signal strength relative to the strength of the noise. The quantity $G_{R,p}(\theta_{i,n}, \phi_{i,n})$ is the antenna gain pattern in the direction of incidence $\theta_{i,n}$ and azimuth $\phi_{i,n}$ angles for the satellite n, the subscript p denotes the polarization of the receiving antenna. The the constant K_n is given by

$$K_n = \frac{P_{T,n} G_{T,n}}{4\pi R_n^2}\left(\frac{\lambda^2}{4\pi}\right) \tag{2}$$

where $P_{T,n}$ and $G_{T,n}$ are the transmitted signal power and gain of the satellite, respectively. The quantity λ is the signal's wavelength, and R_n is the distance between the nth satellite and the ground. The signal measured under the vegetation canopy by the forest unit in Fig. 1 can be written as

$$CN_{0,p}^{F,n} = K_n\left[\gamma_p\left(\theta_{i,n}, \phi_{i,n}\right) G_{R,p}\left(\theta_{i,n}, \phi_{i,n}\right) + S_{M,p}\left(\theta_{i,n}, \phi_{i,n}\right)\right] \tag{3}$$

where $\theta_{i,n}$ and $\phi_{i,n}$ are the incidence and azimuth angles, which are the same as defined in the open area thanks to the gimbal structure. The constant K_n is practically the same as the one in the reference signal since the transmitter is in the mid-Earth orbit (MEO), far away (about 20 000 km) from both receivers. In addition, the atmospheric effects will negligible due to the almost same field of view of the receivers and longer operating wavelength at L-band. The quantity, $\gamma_p(\theta_{i,n}, \phi_{i,n})$ is the transmissivity, which is the parameter of interest to be estimated and represents direct line-of-sight attenuation. The additional term (i.e., $S_{M,p}(\theta_{i,n}, \phi_{i,n})$) in brackets represents the multipath that might happen due to the vegetation–ground interaction and volume scattering within the antenna's field of view.

Taking the ratio of simultaneous measurements of forest and open-sky signals (or logarithmic difference) leads to the cancelation of the common factor K_n for each satellite, but a residual term will remain due to the multipath as

$$\mathrm{Q}_{p,n} = \frac{CN_{0,p}^{F,n}}{CN_{0,p}^{G,n}} = \gamma_p\left(\theta_{i,n}, \phi_{i,n}\right) + \Delta\gamma_p\left(\theta_{i,n}, \phi_{i,n}\right) \tag{4}$$

where the residual term is given by

$$\Delta\gamma_p\left(\theta_{i,n}, \phi_{i,n}\right) = \frac{S_{m,p}\left(\theta_{i,n}, \phi_{i,n}\right)}{G_{r,p}\left(\theta_{i,n}, \phi_{i,n}\right)}. \tag{5}$$

This residual term is expected to be a function of the system (i.e., frequency, polarization, and observation angle) and environmental factors (i.e., tree type, height, density, and gap size). In this article, we will experimentally demonstrate that the impact of forest–ground interaction is mostly negligible, while additional considerations are required for the forest volume scattering as it blends with direct attenuated signal. For simplicity, we will neglect the residual term in (5) when we estimate the VOD values as currently done in most GNSS-T studies [35], [37], [38].

The ratio is then assumed to be equal to the transmissivity that is related to the VOD as

$$\tau_{p,n} = -\ln\gamma_p\left(\theta_{i,n}, \phi_{i,n}\right)\cos\left(\theta_{i,n}\right) \tag{6}$$

where $\tau_{p,n}$ refers to the estimated VOD in the forest.

B. Experimental Plan and Overview

As illustrated in Fig. 1, the forest unit is attached to a UGV platform. Since the goal is to sense the vegetation with the mobile receiver, any signals coming from the ground are undesirable and can impact the measurement accuracy as the rover traverses the forest canopy. First, we studied the impact of ground multipaths on the mobile measurements. For this purpose, we conducted several experiments using smartphone receivers on stationary platforms that involved the collection of GNSS data with different ground plate sizes, and EM absorbers [44]. Finally, we implemented a UGV-based system using custom receivers (e.g., u-blox board) to demonstrate how the GNSS-T concept works with respect to fluctuations within and across tree species and seasonal variations in vegetation. Data collection for this study occurred from February 2020 to June 2021, utilizing different setups involving smartphone receivers and custom GNSS

DATE	18" Ground Plate		12" Ground Plate					
	Phone C	Phone D	Phone C	Phone D	Phone C	Phone D	UBOLX	
2-Feb-2020	FOREST			OPEN				NO ABSORBER
3-Feb-2020		FOREST	OPEN					
7-Feb-2020	OPEN			FOREST				
8-Feb-2020		OPEN	FOREST					
27-Feb-2020						FOREST		ABSORBER
28-Feb-2020						OPEN		
29-Feb-2020				FOREST				
1-Mar-2020				OPEN				
22-Mar-2021							FOREST	MOVING ROVER
22-Mar-2021							OPEN	
19-Apr-2021							FOREST	
19-Apr-2021							OPEN	
20-May-2021							FOREST	
20-May-2021							OPEN	
16-Jun-2021							FOREST	
16-Jun-2021							OPEN	

Fig. 2. Data collected using smartphone receiver as well as u-blox receiver with variable ground plate, platform, and absorber including open sky data and forest data.

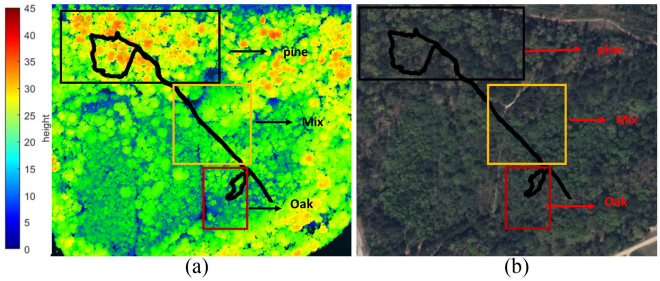

(a) (b)

Fig. 3. (a) LIDAR image of experiment site showing the variation of tree height on the color bar inside the area. The three boxes differentiate the pine, oak, and mixed tree part of the forest with the path of the UGV on it (b) satellite image showing the site where the experiment has been conducted with the path of the UGV on it.

receivers. The comprehensive dataset collected throughout the specified time period is presented in Fig. 2, detailed in the next section.

C. Site Description

The UGV experiments took place within the forested area in the Center for Advanced Vehicular Systems (CAVS) Proving Ground which is a center-wide resource for development and testing of vehicular technology. This area was well surveyed, including airborne (light detection and ranging) LIDAR measurements. Airborne LIDAR data of the site are shown in Fig. 3(a). The point cloud images offered detailed information about the forested region, enabling the estimation of tree heights. These estimations were further compared with satellite images Fig. 3(b). The data proved useful in distinguishing different types of trees within the forested area where the experiment took place. The entire experiment zone has been divided into three parts. The first zone consists of medium-height oak trees, the second zone comprises medium-height mixed deciduous trees, and the third tree zone has large pine trees, as shown in Fig. 3(a).

In addition, we collected diameter at breast height (DBH) data within the oak and pine sites. An area of 30 × 30 m was chosen within the Oak tree sector for detailed examination. The total count of trees possessing a DBH equal to or exceeding ≥3 cm was recorded within this designated area. Subsequently, the DBH of each individual tree within the demarcated 30 × 30-m region was measured. Similarly, within the pine tree sector, a demarcated area measuring 40 × 40 m was selected for investigation. All trees with a DBH of ≥7 cm were enumerated within this chosen area. The DBH of each pine tree located within the specified region was measured. Moreover, using airborne LIDAR measurements, the average height of both oak and pine trees was estimated. Comprehensive tabulation of the DBH measurements is presented in Table I.

TABLE I
IN-SITU DATA WERE GATHERED FROM MARCH TO JUNE WITHIN THE PINE AND OAK FORESTS SEPARATELY

Tree Type		Pine	Oak
Location		33.476591 N 88.791544 W	33.475839 N 88.790804 W
Scan Area (m^2)		1600	900
Number of trees Sampled		155	151
Tree Density($\#/m^2$)		0.097	0.168
DBH (cm)	**Min**	7	3
	Max	97	36
	Mean	26.7	15.07
	SD	20.4	7.5
Height (m)	**Mean**	28.9	12.1
	SD	2.8	1.7

D. Instrumentation

For initial experiments (described in the next section), we utilized two identical smartphones to investigate the multipath effects on the GNSS-T measurements. During the experiment campaign, we also tested the performance of the smartphone in-built antennas. The result of such a study was reported in another study [40], and the conclusion was that the radiation pattern of the smartphone's GNSS antenna is observed to be highly irregular. Thus, we decided to use custom GNSS receivers for the UGV experiments since the irregular antenna pattern can cause discrepancies between reference and mobile receiver measurements, even if a gimbal system is utilized.

1) Smartphone GNSS Receiver Preparation: Two identical smartphones running the Android Oreo operating system (Xiaomi MI8) were utilized. GNSS raw data were collected and stored in receiver-independent exchange format (RINEX) with a one-second sampling rate using an Android app called rinexON, which is freely available at the Google Play store. This work has become possible thanks to direct access to raw GNSS data from mass-market devices running the Android Nougat (or newer) operating system, which was made available in 2016 [45]. A tripod with circular ground plates measuring 12 in (30.48 cm) and 18 in (45.72 cm) in diameter was utilized in the experiment. These ground plates were covered with silver tape, which isolated the reflected ground multipath from the direct signal. The smartphones were identified as Phone-A and Phone-B, respectively, ensuring consistent and comparable measurements

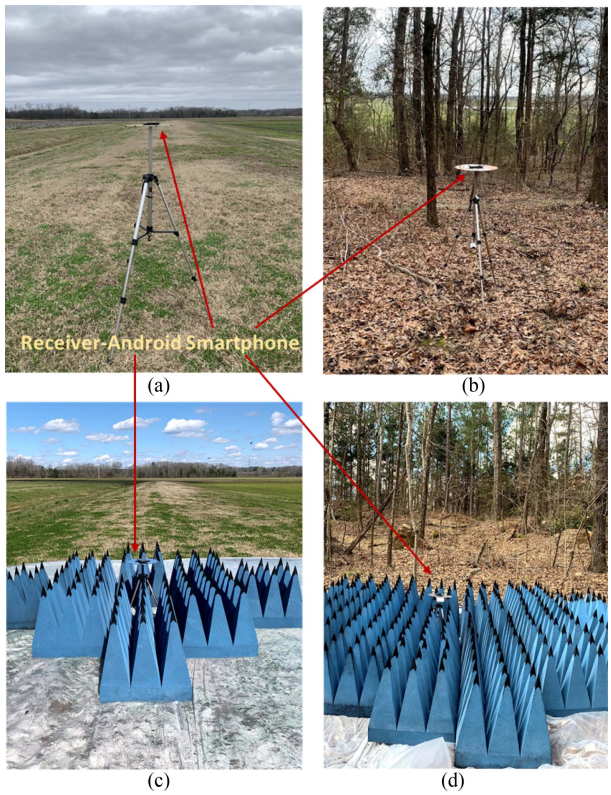

Fig. 4. (a) Smartphone receiver setup with tripod and ground plate to collect data (a) in an open area with no vegetation or scatterer (b) in a forested area with vegetation (c) in an open area with EM absorbers on the ground (d) in a forest area with EM absorbers on the ground to block ground multipath.

throughout the experiment. Fig. 4 shows pictures of the receiver setup in the forest and outside.

2) U-Blox Receiver Preparation: For the mobile GNSS experiment, a custom GNSS receiver utilizing the u-blox ZED-F9P application board was employed. The receiver was accompanied by the AA.175 – Magma X linear polarized omnidirectional GNSS antenna. To facilitate data recording and storage, the receiver was connected to a mini-computer running specialized software known as u-Center. The received signals were recorded and stored within the storage capacity of the onboard computer. Two identical u-blox receivers and antennas were utilized to gather data in both open areas and forested regions, ensuring consistent and comparative measurements. Fig. 5 shows pictures of the stationary reference unit placed on the ground in an open area and the other one mounted on the UGV system under the forest.

3) UGV Preparation: A sturdy UGV, as depicted in Fig. 5(b), was specially designed with the capability to navigate effortlessly through challenging terrains within forested areas. The UGV incorporates the Pixhawk ArduRover UGV control system as its foundation. To ensure optimal performance, the UGV is equipped with a heavy-duty three-axis gimbal, which maintains a level orientation of the receiver with respect to the surface. This gimbal also ensures that the mobile receiver maintains the same orientation as the stationary receiver at all times. Also, a lithium-polymer battery (LiPo) has been used for long-duration experiments.

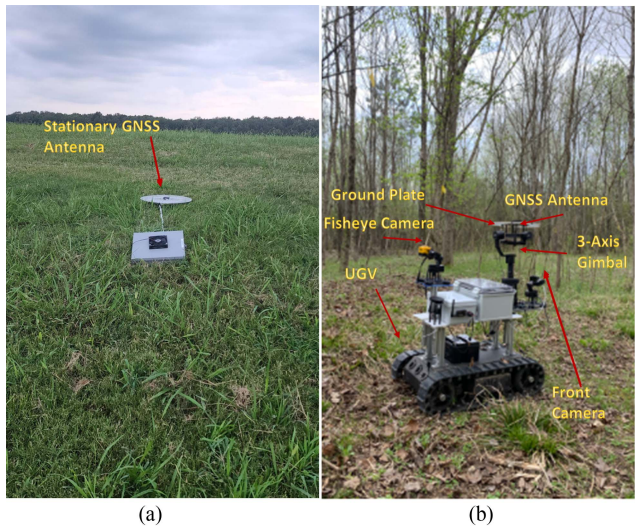

Fig. 5. (a) Stationary u-blox receiver setup to collect data in open sky area without any vegetation or scatterer. It was intentionally placed on ground to ensure no multipath interference affects the reference signal. (b) Custom UGV configured with u-blox receiver setup to collect data under forest area with the front camera, fisheye camera, and three-axis gimbal to keep the GNSS receiver in a fixed orientation.

The UGV is outfitted with a wide-angle lens GoPro camera facing forward, capturing the surroundings along the UGV's driving path. Furthermore, an upward-facing fisheye camera is installed, which records hemispherical images of the forest canopy. Hemispherical photos are used to show seasonal variation in trees due to changes in VWC.

E. Experiment Design

Our working hypothesis is that the multiple scattering involving ground reflections are negligible under the forest canopy, so the UGV-based GNSS receiver collects mainly attenuated and scattered signal within the vegetation. In early 2020, we conducted several experiments to demonstrate the feasibility of this approach under a moving platform and to address the multipath assumption. The summary of the experiments that we conducted is given in Fig. 2. Following the multipath experiment, we conducted a UGV-based experiment on multiple days in the spring and early summer of 2021 to demonstrate how the GNSS-T concept works with respect to signal variations within and across tree species and seasonal changes in VWC. The pictures from these experiments are provided in Figs. 4 and 5. The design of these experiments is briefly described as follows.

1) Multipath Experiment: We designed two distinct experiments to understand the impact of ground multipath on the received signals under the forest by using different ground plate sizes and EM absorbers. Using two smartphones, the experiment took place over multiple days, spanning about a month. In all cases, we had two stationary measurement systems: 1) one receiver on top of a ground plate attached to the tripod in an unobstructed field and 2) the other one on top of a ground plate attached to another tripod under the forest. Both receivers are leveled and oriented in the same direction and recorded the signals simultaneously for approximately 6 h. We used two different ground plate sizes (i.e., 12 inches and 18 inches) to see if

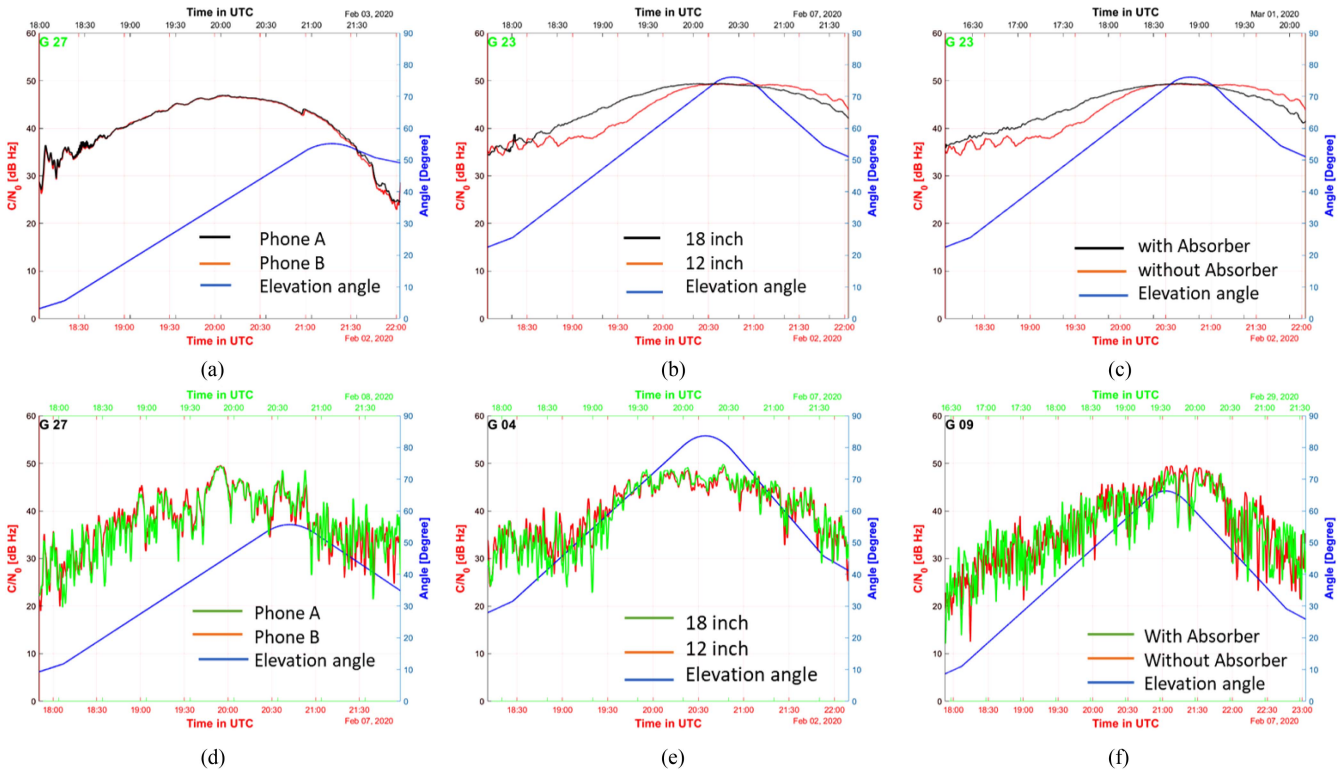

Fig. 6. Signal strength using smartphone receiver (a) in open area with phone A and phone B for GP27 satellite showing the impact of different receiver in open area (b) in open area with 12-inch and 18-inch ground plate for GP23 satellite showing the impact of ground plate size on received signal in open area (c) with and without absorber in open area for GP23 satellite showing the impact of ground multipath in open area (d)in forest area with phone A and phone B for GP27 satellite showing the impact of different receiver in forest area (e) in forest area with 12 in and 18 in ground plate for GP04 satellite showing the impact of ground plate size on received signal in forest area (f) with and without absorber in forest area for GP09 satellite showing the negligible impact of ground multipath in forest area.

the size of the ground plate impacts the measurement. Finally, we covered the ground with absorbers to block the ground reflection completely.

2) Mobile Receiver Experiment: Identical off-the-shelf u-blox GNSS receivers and L-band GNSS antennas were employed to collect signals in both open-sky [see Fig. 5(a)] and under-canopy conditions [see Fig. 5(b)] since smartphones are not appropriate to use on moving platforms because of their irregular antenna patterns, as previously stated. The UGV, equipped with a gimbal and a GNSS receiver, traversed through the forested region while continuously collecting GNSS signals with a full 1000-ms duty cycle. The time-synchronized signals from these stationary and mobile units were then compared, and the difference between them was utilized to calculate the VOD values. Throughout this traversal, the UGV encountered the three specified tree zones: 1) oak trees, 2) pine trees, and 3) mixed trees, as shown in Fig. 3. We repeated the same experiment on four different days in the spring and early summer to investigate the GNSS-T approach's ability to capture seasonal variations.

III. Results

A. Impact of Receiving Systems and Ground Multipath

This analysis involved using two different (but the same model) smartphones to collect data on multiple days from February to March in 2020, focusing on studying the impact of ground multipaths on the GNSS measurements in forest areas. In the analysis, we chose GPS satellites as they have a revisit time of approximately 11 h and 56 min, facilitating comparison of the same satellite configuration quickly. In other words, the different dated data can simply be shifted accordingly to compare the results. It is important to note that the results presented below are specific to a subset of GPS satellites chosen for illustrative purposes, and similar findings were observed for the other available GPS satellites but are not shown here.

Two identical phones (labeled as Phones A and B) are utilized on multiple days to assess consistency over different days and across phones of the same model. This is particularly important as the GNSS-T methodology involves two simultaneous measurements and requires the receivers and configurations to be identical. Fig. 6(a) and (d) show examples of how signal strength changes over time in both forested and open areas. It is evident that the receptions from two identical phones exhibit nearly identical trends under both forest and open areas. This observation indicates that antenna and system-related effects are minimal when two identical receivers are utilized in the GNSS-T methodology. Furthermore, it is evident that the forest signal [see Figs. 6(d)] fluctuates strongly, indicating that the multipath is much stronger compared to the received signals in the open area [see Fig. 6(a)]. In our next step, we aim to delve deeper into the investigation of the predominant source of the multipath interference observed in the forest environment.

This will involve conducting experiments with various ground plate sizes and absorbers to systematically test and analyze their impact on mitigating the ground reflection.

First, we repeated the experiment with different sizes of ground plates (i.e., 12- and 18-in diameter circular plates). The results on February 2nd and February 7th are presented in Fig. 6(b) and (e), respectively. As expected, the size of the ground plate made a notable impact on the received signal in an open area [see Fig. 6(b)]. Conversely, its impact was minimal in the forested area [see Fig. 6(e)], suggesting that the signals primarily came from the upper hemisphere, with ground reflections playing a minor role in the forest.

Finally, to further verify earlier observations, we introduced absorbers on the forest floor from February 27th to March 1st. The comparison of the data with and without absorbers is presented in Fig. 6(c) and (f). Fig. 6(c) shows a significant change in signal strength in the open area that can be attributed to the presence of strong multipath interference as the absorbers are expected to cancel the multipath. In contrast, the signal fluctuations shown in Fig. 6(f) remained very similar, and there was no significant impact of the absorbers on the received signal in the forested area. This can be attributed to the insignificance of ground multipath interference in forested areas. This result reinforces our hypothesis that the multipath due to the ground reflections is indeed insignificant under forest canopies.

The observations presented in these experiments can be summarized as follows.

1) When employing the GNSS-T methodology with two identical receivers configured the same way, antenna and system-related effects are minimal, so the GNSS-T observable [i.e., the ratio in (4)] primarily conveys information about the environment rather than being influenced by instrument and configuration discrepancies.
2) When the mobile forest unit (with an upward-facing GNSS antenna on a ground plate) traverses through a forested area, it captures signals primarily from the forest canopy, irrespective of ground conditions. This effectively results in sampling the forest canopy rather than the ground itself.

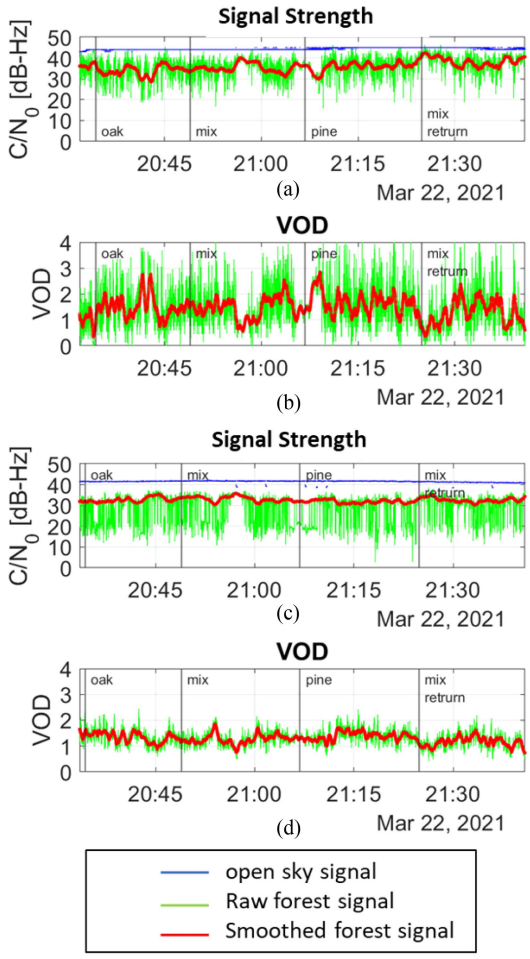

Fig. 7. Temporal variations of both the open sky and forest signals were observed throughout the entire data collection period. In (a), depicting data from Satellite GA-13 in March, the open sky signal (blue line) exhibited greater stability over time, while the forest signal (green line) displayed noticeable fluctuations, albeit consistently smaller than the open sky signal. To mitigate these fluctuations, a moving average with a 45-s window was applied to the forest signal (red line). In (b), the difference between the open and forest signals is illustrated, with the green line representing the difference and the red line indicating the filtered signal using the same moving average window. Notably, the difference is consistently positive due to forest attenuation. (c) presents the time average of all satellites combined over the entire period in an open sky area (blue line), the forest signal (green line), and the moving average of the signal (red line). Finally, in (d), the difference between the sky and forest signals from (c) is shown in the green line, while the red line represents the moving average of the signal.

B. Insights Into the VOD Variations

In the typical GNSS-T configuration, as outlined in Section II, the receiver mounted on a UGV travels randomly under the canopy by visiting the previously identified sites. During such data collection, the many satellites are in the view of the receiver, positioned in various locations in the sky, and moving, but relatively slower. Both motions introduce various observing geometries that lead to fluctuations in the received signal. These fluctuations will be explored in time, space, and angle to provide insights into the complex variations in the received signal in the forested environment.

1) Temporal Variation: The changing positions of the UGV and the satellite influence the received signal significantly in forested areas, while the open sky signal is relatively stable over time as it is unaffected by interference, as evident in Fig. 7(a). The signal gathered by the forest receiver, which travels inside the forest with the UGV, shows more fluctuations in comparison. This is due to the receiver constantly encountering different parts of the forest every second. The raw forest signal has much more variation (in green). So, the signal is averaged with a 45-s moving window (in red) to flatten the signal. As a lower smoothing window cannot remove the interference properly, and a higher moving window can remove the actual features of the signal, a 45-s window is chosen empirically. In addition, the forest signal consistently appears weaker than the open sky signal due to attenuation and scattering caused by the presence of trees. As the transmitter moves considerably slower than the UGV on the ground, the variance in the forest signal is primarily due to the changing view of the forest canopies.

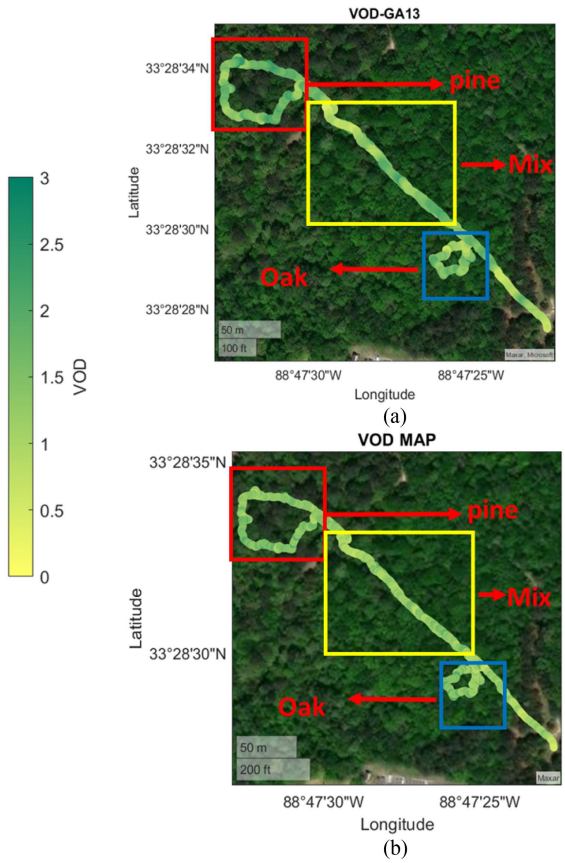

Fig. 8. Spatial variation for (a) GA-13 satellite showing the VOD value over the path followed by the UGV including the pine, oak, and mixed forested area. (b) Spatial averaging of all the satellites over the entire path showing the overall VOD variation as the UGV moves through the forest in the month of March.

Fig. 7(b) illustrates the time average of all the visible satellites throughout the entire time period. The average signal, which takes into account all the satellites, is seen to fluctuate less than individual satellites. This is due to the fact that the variable forest structure and density has a greater impact on the average signal than a satellite's particular behavior does.

By analyzing the temporal aspects of the signals, these observations provide insights into the contrasting behavior of open-sky signals and forest signals over time. The dynamic nature of the moving receiver and the shifting forest environment can be attributed to the differences in the forest signals, while the average signal reflects the combined influence of all satellites and the changing structure of the forest scenario.

2) Spatial Variation: The VOD variations are examined in space to illustrate how the VOD varies as the UGV travels through various vegetation densities or structures. By utilizing the difference between the open sky and forest signal strengths, we employed (4) and (6) to calculate the VOD. These VOD values were subsequently overlaid on a map, matching up them with the receiver's latitude and longitude position in Fig. 8. The plotted VOD values encompass the entire experimental region, encompassing oak, mixed, and pine forests. In Fig. 8(a), the VOD plot represents a single satellite, while Fig. 8(b) displays the VOD plot for the entire region, averaging the VOD values obtained from all available satellite data.

It is evident that there exists a noticeable variation in VOD values for each specific point. This variation highlights the heterogeneous nature of the forest terrain. Therefore, relying on a single reference point within the forest using a stationary receiver is insufficient to represent the forest area accurately. The structure of the forest area fluctuates from one location to another, resulting in different VOD values.

3) Angular Variation: This analysis illustrates how the different positions of the satellites, characterized by varying elevation and azimuth angles, affect the interaction of signals with forest vegetation and subsequently impact the calculation of VOD. Four major GNSS constellations represent more than a hundred satellites, about 30 or more of which can be visible at any point and time. Due to the diversity of the GNSS orbits, one can scan most hemispheric views and monitor from a single to a group of trees within the field of view. Such potential is complicated by the patterns of GNSS orbits, which change continuously.

The position of the satellite has a significant effect on VOD. Our empirical observations reveal that satellites with elevation angles below 30° and beyond 60° yield inconsistent signal strengths. When the transmitting satellite is at a very low incidence angle (i.e., high elevation angles), the receiver predominantly measures an unobstructed signal since near-normal incidence provides the shortest path through vegetation canopies. Also, volume scattering around the line of sight can add up to the receiver signal. As a result, signals from satellites with higher elevation angles (above 60°) exhibit increased strength, yielding lower VOD values. Conversely, when the incidence angle is much higher (i.e., lower elevation angles), the signal travels through a longer path in the forest, which leads to a higher path loss. As a result, the forest signal degrades, causing higher VOD values. In the following analysis, signals from satellites with elevation angles below 30° and above 60° were excluded.

Fig. 9 presents the hemispherical distribution of short-term VOD spatial variations in sky plots where each full circle represents an incidence angle ranging from 0°–90°, while the entire circle represents the azimuth angle ranging from 0°–360°. In Fig. 9(a), the variation of VOD values throughout the data collection period in March is illustrated as the transmitting satellite GP-01 moves while Fig. 9(b) presents the collective data from all constellations (including the GLONASS, Beidou, GPS, and Galileo satellites) across the entire data collection period. The circles are filled using a moving average to present a complete overview. The results show the heterogeneity of forest attenuation with respect to angles of observation, while it is mostly observed that an increase in the incidence angle leads to a corresponding increase in the VOD values.

Given the significant variations of VWC and relative water content within different tree components and across species, the result can inform the variability of VOD at a landscape scale. The spatial integration could help to average the heterogeneity and resolve dynamics linked to soil water dynamics.

C. Seasonal Change in VOD

To investigate the long-term (seasonal) variation in estimated VOD, we conducted an analysis using the GNSS-T data

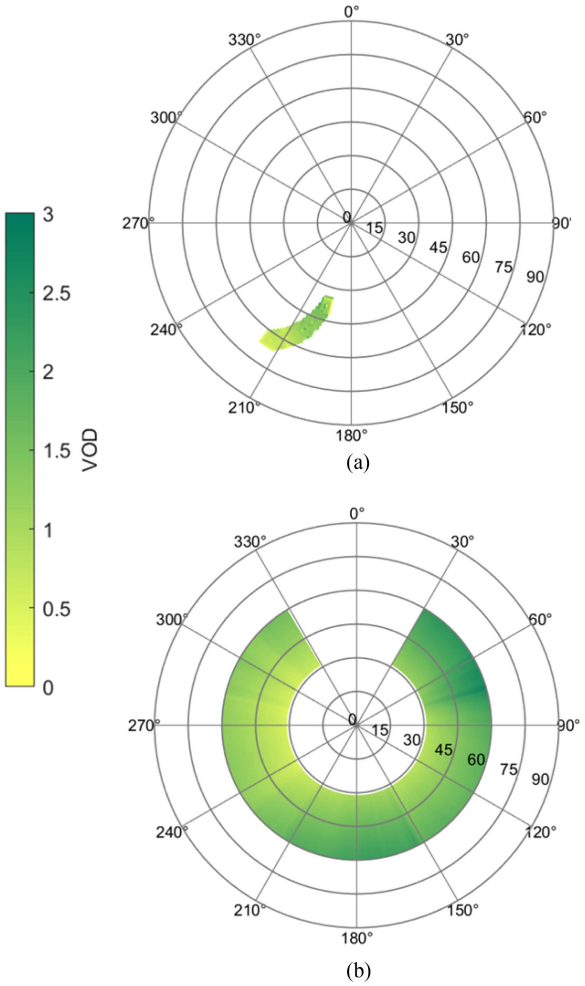

Fig. 9. Angular variation for (a) satellite GP-01 showing the skyplot where each circle represents a different incidence angle and the entire circle represents the azimuth angle. The graph shows the path followed by the specific satellite over the entire data collection period (b), including all the satellites over the entire period. All the data has been moving averaged to show a full representation of the impact of satellite position on VOD measurement.

collected once a month from March to June. Hemispherical images were also taken each month. As seen in Fig. 10, the progressive development of leaves is evident through variations in the greenness and density of leaves, indicating a rise in VWC. The VOD distribution and skyplot are provided in Figs. 11 and 12, respectively. The results show a rise in VOD values throughout the changing of the seasons (from preleaf to leaf-on conditions). The varied vegetation structure that the UGV encounters as it moves through the forest is the cause of the histogram's wider range of values. The same data are depicted in Fig. 12 as skyplots, following the same procedure applied in Fig. 9. Notably, the skyplot transitions from lighter to darker shades as we progress from winter to summer, indicating higher VOD. This highlights the substantial influence of seasonal variations on the overall calculation of VOD. As the vegetation undergoes gradual transformations, the corresponding VOD values also change. The results highlight the significant impact of seasonal changes on the overall VOD calculation, with VOD values fluctuating in response to gradual variations in vegetation.

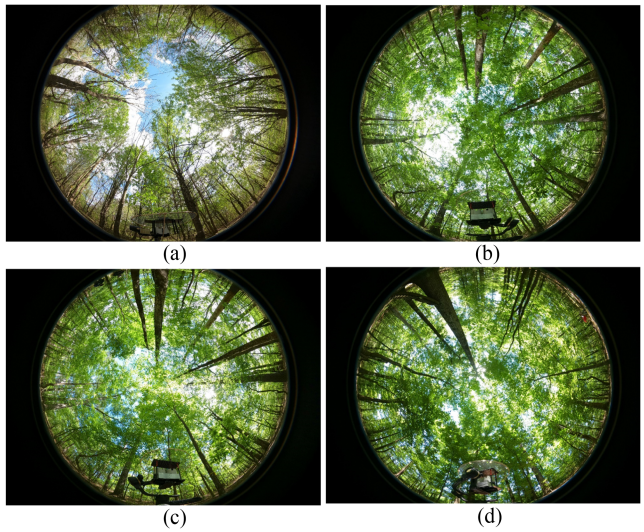

Fig. 10. Skyview of forest from the ground taken with the fisheye camera on the same location in the month of (a) March, (b) April, (c) May, and (d) June to show the variation of tree density of vegetation as the season changes.

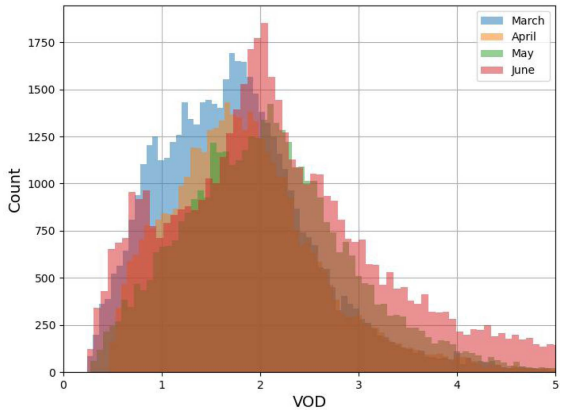

Fig. 11. Histogram depicting the VOD distribution across the entire experiment period is shown for different months: March, April, May, and June. The histogram illustrates the VOD variation as seasonal changes occur. Notably, the VOD values gradually increase from March to June, indicating the transition from winter to summer.

However, the changes are nonuniform but observable. Fig. 13 presents the general trend of VOD values, showcasing a gradual increase from March to June across the entire dataset. Nevertheless, this change is not directly proportional to time, and distinct tree types exhibit visible variations in VOD as the months shift.

D. VOD Variation Across Tree Species

VOD is influenced by the tree species present in the area of interest. Different vegetation kinds have distinctive structures, which causes them to interact with microwave signals in different ways in terms of attenuation and scattering. We split the data into three different plots (i.e., pine, oak, and mixed) to examine how vegetation species affect the VOD estimations. Spatial and angular variations for each plot in May are presented in Fig. 14. The skyplots reveal that oak trees exhibit higher VOD values compared to pine and mixed trees. This can be attributed to

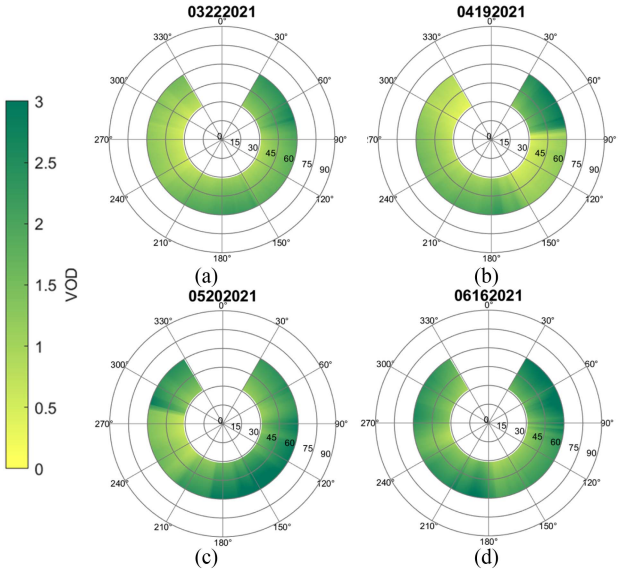

Fig. 12. Angular VOD distribution is presented through skyplots depicting data from all satellites over the entire experiment period for each month: (a) March, (b) April, (c) May, and (d) June. Notably, as we progress from March to May, the VOD values gradually increase, and the skyplots become greener, indicating higher VOD values from March to June.

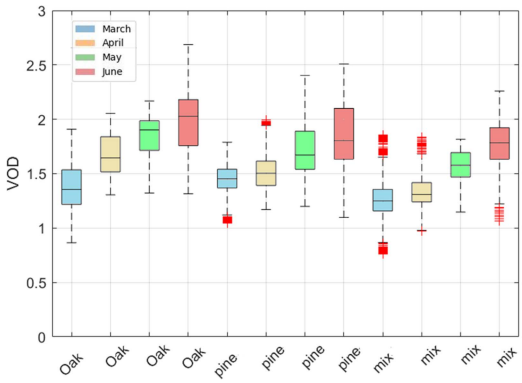

Fig. 13. Distribution of VOD varies across different months for various tree types. As the months advance from March to June, the VOD values for all tree types also increase. This observation illustrates the expected seasonal change for all trees, transitioning from winter to summer.

the higher VOD observed in the oak tree path due to its higher canopy density (see Table I) and, subsequently, higher VWC. It is important to point out that no VWC measurements are made in this study. The higher VWC is expected for oak trees due to their expected higher values of leaf area index (LAI), as evident in Fig. 10. The forest signal is substantially weaker in oak forests compared to pine and mixed forests due to the greater attenuation because of higher VWC. In addition, pine trees have higher VOD values than mixed trees, mostly as a result of their taller height and greater density of needles (higher LAI), both of which contribute to the observed variations in VOD patterns.

The distribution of VOD readings in oak and pine forests during the month of May is shown by the histogram in Fig. 15. The VOD values in the oak forest are noticeably greater than those in the pine forest. This discrepancy can be attributed to the greater vegetation density within the oak forest, leading to a higher water content and, consequently, higher VOD values. Furthermore, Fig. 15 reveals that pine trees exhibit higher VOD values compared to the mixed trees. This difference results from the pine tree's higher density and height, which have more scattering and attenuation effects than mixed trees. As a result, the VOD readings on the pine trees are greater. These trends were consistently observed in all data collection periods as well, indicating the relationship between vegetation density, water content, and VOD measurements in both oak, pine, and mixed forests.

Fig. 16 presents the variations in VOD values for different tree species across various months. Compared to mixed and oak trees, pine trees have greater VOD values in March. This is explained by the fact that oak trees have less leaf density at this time of year, whereas pine trees have taller heights and more needles, which increases VOD values. The leaf density of oak trees greatly increases as the months move toward summer, outpacing that of pine and mixed trees in terms of VOD. As a result, compared to mixed and pine trees, oak trees have much higher VOD values in the months of April, May, and June. The combined impact of seasonal variations and tree species on VOD is clearly depicted in this illustration.

IV. Discussion

This study explored the possibility of remote sensing of forest VOD using low-cost GNSS receivers at landscape scale with one receiver moving under forest while another identical receiver in the open area as reference. This approach, known as GNSS-T, is aimed to measure canopy transmissivity rather than reflectivity, distinguishing it from GNSS reflectometry. To check the effectiveness of this technique, it was crucial to ensure that the sampling focused on vegetation rather than ground as the mobile platform moved randomly through the forest. Specific experiments were conducted involving the placement of absorbers on the ground and the use of various sizes of ground plates. Through these experiments, it was demonstrated that the interaction between the forest and ground was negligible when compared to the scattering and absorption by vegetation. However, additional considerations are required for the forest volume scattering as it blends with direct attenuated signal, adding a residual term to the estimated transmissivity, consequently VOD estimates.

Guerriero et al. [36] applied a theoretical scattering model to a poplar forest and provided some insights into the source of scattering within the canopy. They showed that only the left-hand circular polarized signals, which the majority of geodetic ground-based GNSS antennas are designed to reject, are dominated by volume scattering and the right-hand circular polarized GNSS signals measured below a forest canopy are dominated by coherent attenuation. However, further research is needed from modeling perspective to better understand the impact of the residual term on the VOD estimates to expand these results to different forest types, densities, and heights. In particular, more considerations are needed for canopy architecture, gaps, large scatterers, different polarization (e.g., linear polarized antennas), and observation angles [46], [47].

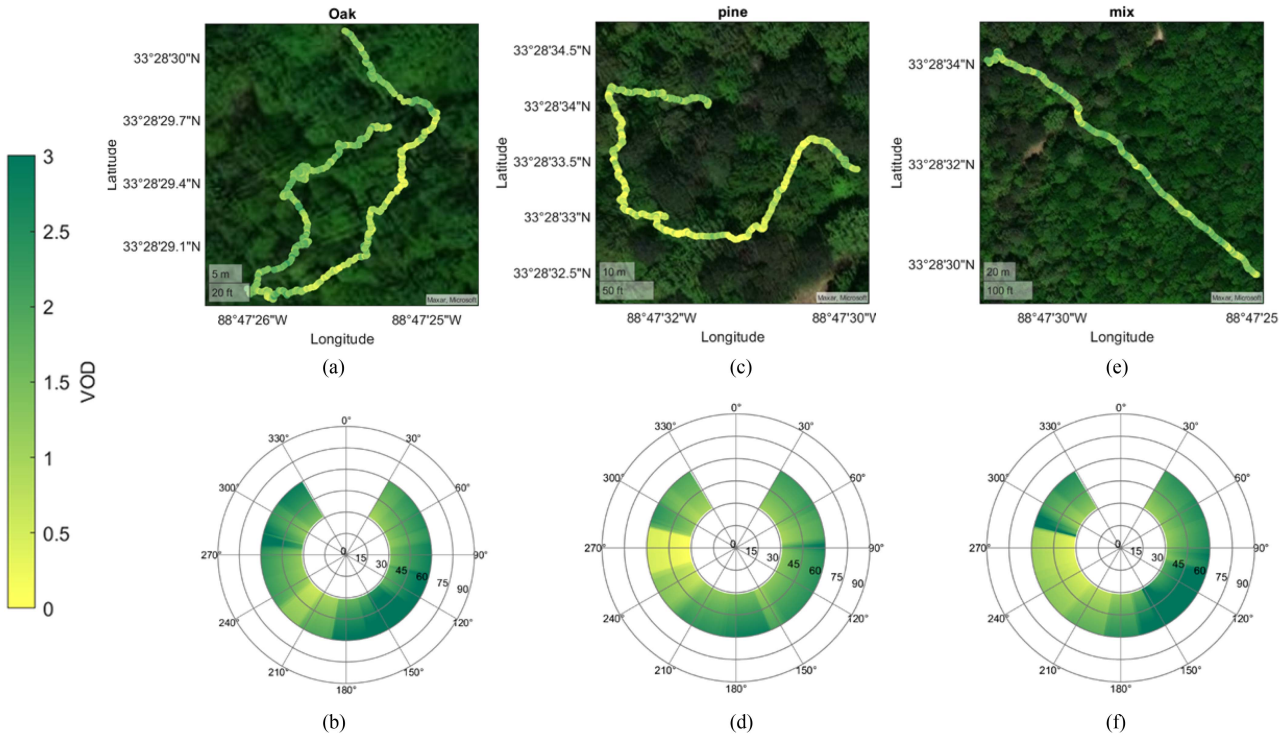

Fig. 14. VOD variation is demonstrated for three distinct plots of trees in the forest area. VOD maps over the oak, pine, and mixed forests are shown as the UGV traverses through each forest region, represented by (a), (c), and (e), respectively. In addition, (b), (d), and (f) illustrate the skyplots of the oak, pine, and mixed forests, respectively, in the month of May. Notably, the highest VOD values are observed in the Oak forest, followed by the pine trees and then the mixed trees. This indicates that the VOD value varies among different types of trees.

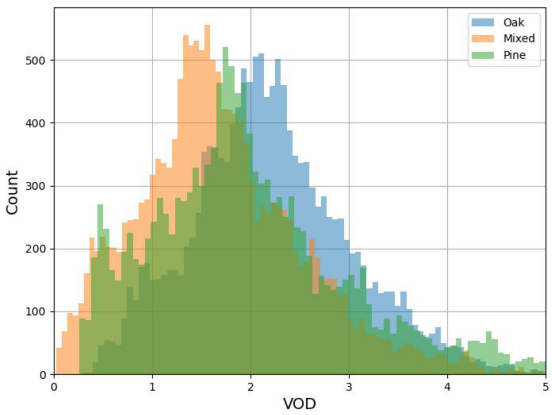

Fig. 15. Histogram illustrates the VOD distribution in different types of trees. Compares the VOD distribution between oak, mixed, and pine trees in the month of May. Observations reveal that oak trees exhibit higher VOD values compared to pine trees.

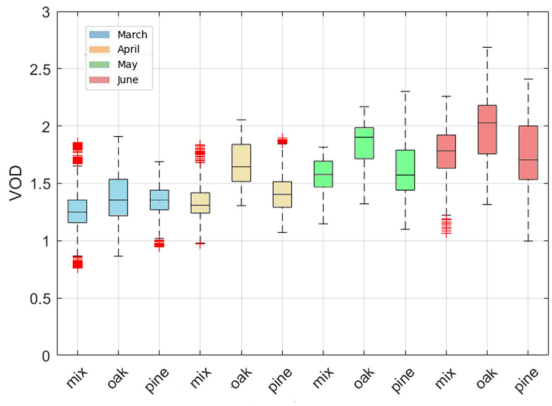

Fig. 16. VOD distribution of different tree types in different months is examined. In March, oak trees exhibited lower VOD values similar to pine and mixed trees. However, as the months progress, Oak trees demonstrate a rapid increase in VOD values, surpassing both Pine and mixed trees. Eventually, oak trees show higher VOD values than pine and mixed trees.

In this study, we collected mobile GNSS-T data over oak, pine, and mixed trees on multiple days in the spring and early summer of 2021. The data indicated an increase in VOD values correlating with seasonal variations, which were captured by fish-eye cameras. However, due to the absence of in-situ VWC measurements, a direct comparison between VOD and VWC was not presented in the article. In addition, the VOD estimates can depend also on many factors including plant height, density, structure, and age. In our study area, we did not have sufficient site diversity to investigate such relations. For instance, oak trees are denser than pine trees, but they are shorter than pine trees (see Table I). Overall, we did not observe a large difference in VOD except timing of seasonal changes in VOD estimates. In fact, with a similar GNSS-T setup and more than 20 sites, we recently collected a more diverse dataset in conjunction with airborne and terrestrial LiDAR during SMAP validation experiments (SMAPVEX) in temperate forests [48]. This can allow to validate and further explain the VOD measurements with more in-situ data from the SMAPVEX field campaign. Future studies can include investigation of determining the best

geophysical parameters (e.g., woody volume, crown diameter, shape, and plant area density) to describe the VOD. Moreover, determining the specific vegetation layers that influence the measurement would be beneficial. Ultimately, establishing the relationship between VOD and VWC remains a crucial future objective.

V. Conclusion

In this article, we conducted an empirical study on mobile GNSS-T measurements, yielding several key findings. First, we investigated the influence of ground multipath on the GNSS-T measurements, revealing minimal impact on the received signal under the forest canopy. This means that the mobile forest unit, equipped with an upward-facing GNSS antenna on a ground plate, effectively samples the forest canopy rather than the ground itself. Second, we illustrated how the mobile forest unit captures the heterogeneity of the forest. Third, we emphasized the crucial role of the transmitting satellite's position in influencing VOD measurements. Fourth, an examination of seasonal changes showed a positive correlation between VOD and seasonal progression in the forest's hydrological state. Finally, we explored VOD variations across different tree species and presented evidence supporting a strong correlation between estimated VOD and VWC through optical measurements of vegetation. These findings collectively contribute to an understanding of the interactions between GNSS-T measurements and forest conditions. Further studies, in particular theoretical studies, are needed to understand better the relative value of configurational parameters (e.g., elevation angle, polarizations) and the optimal design of VWC retrieval algorithms.

GNSS-T offers an opportunity to sample vegetation more comprehensively than current in-situ systems. With the help of this technology, larger forested areas can be covered in a shorter amount of time, giving a larger view of the forest ecosystems. Moreover, GNSS-T can capture variations within forested regions due to the heterogeneous structure of the forests. While it may not yield information on the diurnal cycle of vegetation, it can be a valuable tool for regular monitoring and understanding long-term changes in the forest environment.

References

[1] A. G. Konings et al., "Detecting forest response to droughts with global observations of vegetation water content," *Glob. Change Biol.*, vol. 27, no. 23, pp. 6005–6024, 2021.

[2] A. D. Richardson, T. F. Keenan, M. Migliavacca, Y. Ryu, O. Sonnentag, and M. Toomey, "Climate change, phenology, and phenological control of vegetation feedbacks to the climate system," *Agricultural Forest Meteorol.*, vol. 169, pp. 156–173, 2013.

[3] R. Buitenwerf, L. Rose, and S. I. Higgins, "Three decades of multi-dimensional change in global leaf phenology," *Nature Climate Change*, vol. 5, no. 4, pp. 364–368, 2015.

[4] X. Ma, A. Huete, S. Moran, G. Ponce-Campos, and D. Eamus, "Abrupt shifts in phenology and vegetation productivity under climate extremes," *J. Geophys. Res.: Biogeosci.*, vol. 120, no. 10, pp. 2036–2052, 2015.

[5] D. Touma, M. Ashfaq, M. A. Nayak, S.-C. Kao, and N. S. Diffenbaugh, "A multi-model and multi-index evaluation of drought characteristics in the 21st century," *J. Hydrol.*, vol. 526, pp. 196–207, 2015.

[6] M. T. Tyree and J. S. Sperry, "Vulnerability of xylem to cavitation and embolism," *Annu. Rev. Plant Biol.*, vol. 40, no. 1, pp. 19–36, 1989.

[7] P. Gentine, M. Guérin, M. Uriarte, N. G. McDowell, and W. T. Pockman, "An allometry-based model of the survival strategies of hydraulic failure and carbon starvation," *Ecohydrology*, vol. 9, no. 3, pp. 529–546, 2016.

[8] P. O'Neill et al., "Comrad active/passive microwave measurement of tree canopies," in *Proc. IEEE Int. Geosci. Remote Sens. Symp.*, 2007, pp. 1420–1423.

[9] P. Ceccato, S. Flasse, and J.-M. Gregoire, "Designing a spectral index to estimate vegetation water content from remote sensing data: Part 2. validation and applications," *Remote Sens. Environ.*, vol. 82, no. 2-3, pp. 198–207, 2002.

[10] T. J. Jackson et al., "Vegetation water content mapping using landsat data derived normalized difference water index for corn and soybeans," *Remote Sens. Environ.*, vol. 92, no. 4, pp. 475–482, 2004.

[11] A. G. Konings, K. Rao, and S. C. Steele-Dunne, "Macro to micro: Microwave remote sensing of plant water content for physiology and ecology," *New Phytologist*, vol. 223, no. 3, pp. 1166–1172, 2019.

[12] H. Wang et al., "Seasonal variations in vegetation water content retrieved from microwave remote sensing over amazon intact forests," *Remote Sens. Environ.*, vol. 285, 2023, Art. no. 113409.

[13] V. Barraza et al., "Monitoring vegetation moisture using passive microwave and optical indices in the dry Chaco forest, Argentina," *IEEE J. Sel. Topics Appl. Earth Observ. Remote Sens.*, vol. 7, no. 2, pp. 421–430, Feb. 2013.

[14] Y. Zhang, S. Zhou, P. Gentine, and X. Xiao, "Can vegetation optical depth reflect changes in leaf water potential during soil moisture dry-down events?," *Remote Sens. Environ.*, vol. 234, 2019, Art. no. 111451.

[15] G. Vaglio Laurin, C. Vittucci, G. Tramontana, P. Ferrazzoli, L. Guerriero, and D. Papale, "Monitoring tropical forests under a functional perspective with satellite-based vegetation optical depth," *Glob. Change Biol.*, vol. 26, no. 6, pp. 3402–3416, 2020.

[16] F. Frappart et al., "Global monitoring of the vegetation dynamics from the vegetation optical depth (VOD): A review," *Remote Sens.*, vol. 12, no. 18, 2020, Art. no. 2915.

[17] N. M. Holtzman et al., "L-band vegetation optical depth as an indicator of plant water potential in a temperate deciduous forest stand," *Biogeosciences*, vol. 18, no. 2, pp. 739–753, 2021.

[18] M. Momen et al., "Interacting effects of leaf water potential and biomass on vegetation optical depth," *J. Geophys. Res.: Biogeosci.*, vol. 122, no. 11, pp. 3031–3046, 2017.

[19] F. Tian et al., "Coupling of ecosystem-scale plant water storage and leaf phenology observed by satellite," *Nature Ecol. Evol.*, vol. 2, no. 9, pp. 1428–1435, 2018.

[20] J.-P. Wigneron et al., "SMOS-IC data record of soil moisture and L-VOD: Historical development, applications and perspectives," *Remote Sens. Environ.*, vol. 254, 2021, Art. no. 112238.

[21] A. G. Konings, M. Piles, N. Das, and D. Entekhabi, "L-band vegetation optical depth and effective scattering albedo estimation from smap," *Remote Sens. Environ.*, vol. 198, pp. 460–470, 2017.

[22] J. Du, J. S. Kimball, L. A. Jones, Y. Kim, J. Glassy, and J. D. Watts, "A global satellite environmental data record derived from AMSR-E and AMSR2 microwave Earth observations," *Earth Syst. Sci. Data*, vol. 9, no. 2, pp. 791–808, 2017.

[23] Y. H. Kerr et al., "The SMOS soil moisture retrieval algorithm," *IEEE Trans. Geosci. Remote Sens.*, vol. 50, no. 5, pp. 1384–1403, May 2012.

[24] M. Wang et al., "A consistent record of vegetation optical depth retrieved from the AMSR-E and AMSR2 x-band observations," *Int. J. Appl. Earth Observation Geoinf.*, vol. 105, 2021, Art. no. 102609.

[25] C. Vittucci, L. Guerriero, P. Ferrazzoli, R. Rahmoune, V. Barraza, and F. Grings, "Study of multifrequency sensitivity to soil moisture variations in the lower Bermejo basin," *Eur. J. Remote Sens.*, vol. 46, no. 1, pp. 775–788, 2013.

[26] M. Wang et al., "An alternative AMSR2 vegetation optical depth for monitoring vegetation at large scales," *Remote Sens. Environ.*, vol. 263, 2021, Art. no. 112556.

[27] C. Vittucci et al., "SMOS retrieval over forests: Exploitation of optical depth and tests of soil moisture estimates," *Remote Sens. Environ.*, vol. 180, pp. 115–127, 2016.

[28] C. Vittucci, G. V. Laurin, G. Tramontana, P. Ferrazzoli, L. Guerriero, and D. Papale, "Vegetation optical depth at L-band and above ground biomass in the tropical range: Evaluating their relationships at continental and regional scales," *Int. J. Appl. Earth Observation Geoinf.*, vol. 77, pp. 151–161, 2019.

[29] C. Vittucci, L. Guerriero, and P. Ferrazzoli, "Influence of vegetation height, plant area index and forest intactness on SMOS L-VOD, for different seasons and latitude ranges," *IEEE Trans. Geosci. Remote Sens.*, vol. 61, 2023, Art. no. 5301911.

[30] N. J. Rodríguez-Fernández et al., "An evaluation of SMOS l-band vegetation optical depth (L-VOD) data sets: High sensitivity of L-VOD to above-ground biomass in africa," *Biogeosciences*, vol. 15, no. 14, pp. 4627–4645, 2018.

[31] A. Mialon et al., "Evaluation of the sensitivity of SMOS L-VOD to forest above-ground biomass at global scale," *Remote Sens.*, vol. 12, no. 9, 2020, Art. no. 1450.
[32] H. Carreno-Luengo, G. Luzi, and M. Crosetto, "Above-ground biomass retrieval over tropical forests: A novel GNSS-R approach with CyGNSS," *Remote Sens.*, vol. 12, no. 9, 2020, Art. no. 1368.
[33] E. Santi et al., "Remote sensing of forest biomass using GNSS reflectometry," *IEEE J. Sel. Topics Appl. Earth Observ. Remote Sens.*, vol. 13, pp. 2351–2368, 2020.
[34] A. Colliander et al., "SMAP detects soil moisture under temperate forest canopies," *Geophys. Res. Lett.*, vol. 47, no. 19, 2020, Art. no. e2020GL089697.
[35] V. Humphrey and C. Frankenberg, "Continuous ground monitoring of vegetation optical depth and water content with GPS signals," *Biogeosciences*, vol. 20, no. 9, pp. 1789–1811, 2023.
[36] L. Guerriero et al., "Ground-based remote sensing of forests exploiting GNSS signals," *IEEE Trans. Geosci. Remote Sens.*, vol. 58, no. 10, pp. 6844–6860, Oct. 2020.
[37] N. Rodriguez-Alvarez et al., "Vegetation water content estimation using GNSS measurements," *IEEE Geosci. Remote Sens. Lett.*, vol. 9, no. 2, pp. 282–286, Mar. 2012.
[38] M. Zribi, E. Motte, P. Fanise, and W. Zouaoui, "Low-cost GPS receivers for the monitoring of sunflower cover dynamics," *J. Sensors*, vol. 2017, 2017, Art. no. 6941739.
[39] A. Camps, A. Alonso-Arroyo, H. Park, R. Onrubia, D. Pascual, and J. Querol, "L-band vegetation optical depth estimation using transmitted GNSS signals: Application to GNSS-reflectometry and positioning," *Remote Sens.*, vol. 12, no. 15, 2020, Art. no. 2352.
[40] M. Kurum, A. Gurbuz, and M. M. Farhad, "Gnss reflectometry from smartphones: Testing performance of in-built antennas and GNSS chips," in *Proc. IEEE Int. Geosci. Remote Sens. Symp.*, 2020, pp. 6278–6281.
[41] M. Kurum, M. M. Farhad, and D. Boyd, "Gnss transmissometry (GNSS-T): Modeling propagation of GNSS signals through forest canopy," in *Proc. IEEE Int. Geosci. Remote Sens. Symp.*, 2022, pp. 4695–4698.
[42] H. D. Adams et al., "A multi-species synthesis of physiological mechanisms in drought-induced tree mortality," *Nature Ecol. Evol.*, vol. 1, no. 9, pp. 1285–1291, 2017.
[43] J. Martínez-Vilalta and F. Lloret, "Drought-induced vegetation shifts in terrestrial ecosystems: The key role of regeneration dynamics," *Glob. Planet. Change*, vol. 144, pp. 94–108, 2016.
[44] M. Kurum and M. Farhad, "UGV-based mapping of forest transmissivity using GPS measurements," in *Proc. IEEE Int. Geosci. Remote Sens. Symp.*, 2021, pp. 6076–6079.
[45] S. Malkos, "User location takes center stage in new android os: Google to provide raw GNSS measurements," *GPS World*, vol. 27, no. 7, p. 36, 2016.
[46] S. Yadav, A. Ghosh, D. Boyd, and M. Kurum, "A realistic framework of GNSS-T for simulating scattering and propagation of GNSS signals under a forest canopy," in *Proc. Photon. Electromagn. Res. Symp.*, 2023.
[47] W. Gu, L. Tsang, A. Colliander, and S. Yueh, "Hybrid method for full-wave simulations of forests at L-band," *IEEE Access*, vol. 10, pp. 105898–105909, 2022.
[48] A. Ghosh et al., "Forest vegetation optical depth mapping using GNSS signals at SMAPVEX'22," in *Proc. IEEE Int. Geosci. Remote Sens. Symp.*, 2023, pp. 3237–3240.

Abesh Ghosh (Student Member, IEEE) received the B.Sc. degree in electrical and electronic engineering from the Bangladesh University of Engineering and Technology, Dhaka, Bangladesh, in 2019. He is currently working toward the Ph.D. degree in electrical and computer engineering with the University of Georgia, Athens, GA, USA.

His research interests include unmanned ground vehicle-based GNSS-T techniques for the remote sensing of Earth surface parameters using low-cost and smart devices and modeling of vegetation to understand the effect of microwave signals on forest.

Mr. Ghosh is a student member of the IEEE Geoscience and Remote Sensing Society.

Md Mehedi Farhad (Student Member, IEEE) received the B.Sc. degree in electrical and electronic engineering from the Ahsanullah University of Science and Technology, Dhaka, Bangladesh, in 2012. He is currently working toward the Ph.D. degree in electrical and computer engineering with Mississippi State University, Mississippi State, MS, USA.

He is currently a Research Assistant with the Information Processing and Sensing (IMPRESS) Laboratory. His research interests include investigating Unmanned Aircraft Systems (UAS)-based GNSS-R techniques and Unmanned Ground Vehicle (UGV)-based GNSS-T techniques for the remote sensing of Earth surface parameters using low-cost and smart devices.

Mr. Farhad was the recipient of Future Investigators in NASA Earth and Space Science and Technology award in 2023. He is a student member of the IEEE Geoscience and Remote Sensing Society.

Dylan Boyd (Member, IEEE) received the B.S. and Ph.D. degrees in electrical and computer engineering from Mississippi State University, Mississippi State, MS, USA, in 2017 and 2023, respectively.

He is currently a Research Associate with NASA Goddard Space Flight Center, Greenbelt, MD, USA.

His research interests include the forward and inverse modeling of SoOp-R, SAR, and passive scenarios to establish relationships between microwave remote sensing measurements and Earth science parameters for remote sensing.

Mehmet Kurum (Senior Member, IEEE) received the B.S. degree in electrical and electronics engineering from Bogazici University, Istanbul, Turkey, in 2003, and the M.S. and Ph.D. degrees in electrical engineering from George Washington University, Washington, DC, USA, in 2005 and 2009, respectively.

He held Postdoctoral and Research Associate positions with the Hydrological Sciences Laboratory, NASA Goddard Space Flight Center, Greenbelt, MD, USA. From 2016 to 2022, he served as an Assistant Professor with Mississippi State University (MSU), Mississippi State, MS, USA, and subsequently, he held the position of Associate Professor and the Paul B. Jacob endowed Chair, until 2023. He is currently an Associate Professor of Electrical and Computer Engineering with the University of Georgia, while also serving as an Adjunct Professor with MSU. His research interests include recycling the radio spectrum to address the challenges of decreasing radio spectrum space for science while exploring entirely new microwave regions for land remote sensing.

Dr. Kurum is a member of U.S. National Committee for the International Union of Radio Science. Dr. Kurum was a recipient of the Leopold B. Felsen Award for excellence in electromagnetic in 2013 and URSI Young Scientist Award in 2014, and NSF CAREER award in 2022. He has been an Associate Editor for IEEE TRANSACTIONS ON GEOSCIENCE AND REMOTE SENSING and IEEE JOURNAL OF SELECTED TOPICS IN APPLIED EARTH OBSERVATIONS AND REMOTE SENSING since 2021. He served as an Early Career Representative for the International URSI Commission F (Wave Propagation and Remote Sensing), from 2014–2021. He is a Senior Member of IEEE Geoscience and Remote Sensing Society.